ARAI
Journal of Sensors
Volume 2023, Article ID 2102915, 10 pages https://doi.org/10.1155/2023/2102915

Research Article

Black Phosphorous and Cytop Nanofilm-Based Long-Range SPR Sensor with Enhanced Quality Factor

Bhishma Karki[1,2] **Arun Uniyal**[3] **Gaurav Srivastava**[4] **and Amrindra Pal**[5] [1]

[1] *Department of Physics, Tri-Chandra Multiple Campus, Tribhuvan University, Kathmandu, 44600, Nepal*
[2] *National Research Council Nepal, New Baneshwor-10, Kathmandu, 44600, Nepal*
[3] *Department of ECE, IT Gopeshwar, Chamoli, 246424 Uttarakhand, India*
[4] *Department of Electronics and Communication, University of Allahabad, India*
[5] *Department of ECE, DIT University, Dehradun, 248009 Uttarakhand, India*

Correspondence should be addressed to Bhishma Karki; magnum.photon@gmail.com

Received 19 September 2022; Revised 9 January 2023; Accepted 20 January 2023; Published 6 February 2023

Academic Editor: Qiang Wu

This numerical work proposes two novel designs of long-range surface plasmon resonance sensors (LRSPR) using two different coupling prisms. The performance analysis of the proposed sensor has been investigated using the performance parameters like quality factor (Q), detection accuracy (DA), sensitivity (S), and full-width half maximum (FWHM). The transfer matrix method (TMM) has been employed to compute reflectance. The role of the basic recognition element (BRE) has been played by the popular two-dimensional (2D) material, black phosphorus (BP), due to its many optoelectrical features. The maximum obtained values for Q, DA, and S are 3333.25 ð1/RIUÞ, 250 ðdegree^{-1}Þ, and 13.33333 degree/RIU for 2S2G coupled sensor design and 3055.5 ð1/RIUÞ, 83.33 ðdegree^{-1}Þ, and 36.66667 degree/RIU for BK7 coupled sensor design. The operating wavelength of 633 nm, followed by the principle of attenuated total reflection (ATR), has been employed to carry out the theoretical investigation.

1. Introduction

Over the past decade, many research works have been carried out on various sensing mechanisms. Surface plasmon resonance (SPR) is the mainly focused principle for many sensing applications in the optical field [1]. The surface plasmons (SPs) are the cloud of electrons propagating along the metal surface as the incident wave (TM polarized) strikes the metal surface's free electrons [2, 3]. So, the phenomenon of SPR generally occurs when the incident wave vector matches with the surface plasmon wave vector [4]. SPR sensor design can be classified mainly as prism-based [5], grating-based [6], optical waveguide coupling [7], and fiber-based [8]. From these, the prism and fiber coupling are the most popular SPR structures. In optical materials, the dielectric function of the refractive index is critical for controlling the flow of electromagnetic wave propagation. A significant alteration in the SPR signal can be noted for a slight alteration in the refractive index in the environment. Recent developments in various biosensors make them extensively used in the medical [9], bioengineering [10], environmental [11], and food industries [12]. Higher requirements in terms of sensitivity, specificity, and bioassay methods have been raised due to the evolution of biotechnology. The above requirements are not easy to be fulfilled by the conventional SPR (CSPR). So, some new

SPR modes like long-range surface plasmon resonance (LRSPR), waveguide coupled surface plasmon resonance (WCSPR), and coupled plasmon waveguide resonance (CPWR) have been studied [13]. In the year 1981, Sarid had given the concept of LRSPR [14]. The mechanism of LRSPR is a special electromagnetic (EM) mode in which a layer of dielectric buffer was inserted between metal and the substrate. The long-range surface plasmon penetrates deep inside the analyte because of weaker confinement between the metal layers. As a result, it has a longer propagation distance and greater EM field generation than the CSPR. The EM fields of the surface plasmon polaritons (SPPs) that belong to the two interfaces of the metal layer start to overlap when it is sandwiched between two dielectric layers with the same refractive index (RI), creating a symmetric EM field mode and an antisymmetric EM field mode [13]. The penetration depth in the analyte and propagation length along the interface between the metal film and analyte in the case of symmetric mode is quite higher, with a lower value of attenuation than in the other case. Due to this, the field distribution is symmetric EM field mode for long-range SPPs, while the antisymmetric EM field mode is called short-range surface plasmon resonance. Other advantages of long-range surface plasmon include the greater figure of merit (FOM) and detection accuracy (DA) with a low full-width half maximum (FWHM) [14].

Typical materials employed in sensing applications are noble metals, like silver (Ag) [15] and gold (Au) [16]. Despite these popular plasmonic metals (Ag and Au), other metals, nickel [17], aluminium (Al) [18], copper (Cu) [19], etc., can also be employed for LRSPR-based applications. The traditional sensor based on LRSPR, gold (Au), is generally preferred as the prime plasmonic metal as it has great performance in the visible and near-infrared spectral bands and exceptional chemical stability under ambient circumstances. Still, it cannot process oxidation with lower chemical reactivity. Also, the Au-based SPR sensors show less DA and have inefficient responses in sensing applications [20]. The advantages of using the Ag layer are its sharper/ more intense LRSPR bands compared with Au; its inclusion increases the sensor's sensitivity and low optical loss in the visible and near-infrared (NIR), spectral bands, making it an optimum material for plasmonics. Although its demerits are also there, oxidation problems and considerable losses due to its surface roughness exist [21]. The oxidation problem can be reduced using other 2D materials/semiconductors [22]. Cu and Al become viable alternatives since Ag and Au are too expensive. Cu and Al, however, are chemically unstable in an atmosphere, limiting the scope of their potential uses. Alkali metals are also excellent for sensing applications, but because of their high reactivity to water and air, they must be kept in a vacuum or inert gas during storage [21]. The sensor geometry or configuration used in our proposed design is Kretschmann-Raether-based [23, 24].

The conventional configuration comprises a coupling prism and a metal layer. In between these layers, no air gap is present. Its easy practicability over the other prismcoupled Otto configuration [25] makes it a popular design choice in LRSPR-based sensors. Many interrogation techniques, like wavelength interrogation, angle interrogation, phase interrogation, intensity interrogation, and amplitude interrogation techniques, are available for SPR sensing applications [26, 27]. The angle interrogation technique is employed here. The mechanism of ATR was the prime principle of the proposed sensor.

Many research studies have been done based on the LRSPR phenomenon. Wark et al. [28] reported an LRSPRbio affinity sensor to investigate the hybridization of DNA adsorption and proposed the fabrication steps for the LRSPR chip. Khodami and Berini [29] reported an LRSPR sensor to measure anti-BSA/BSA interaction binding kinetics constants. Wang et al. [30] investigated a grating-based LRSPR sensor to detect E. coli O157: H7 bacteria. They attained a
75.4 deg/RIU sensitivity and a full-width half maximum of 0.65 deg. Fan et al. [31] reported an LRSPR sensor using graphene; they attained higher sensitivity and detection accuracy values. Pandey et al. [32] proposed an LRSPR biosensor using the dielectric buffer layer (DBL), MXene, FG, and analyte layers and attained the highest FOM of 347 (1/RIU).

Following graphene's astounding success, few-layer black phosphorus (BP) has demonstrated its enormous potential in biosensing. Black phosphorus became popular due to its puckered lattice design, high carrier mobility, considerable optical anisotropy, tunable bandgap with effective carrier mass and work function, higher molecular adsorption, and high surface-to-volume ratio [33–35]. The single demerit of BP is its nonstability in air and water. Due to this, it is a perfectly suitable 2D material for gas-based sensors [36].

Cytop is a dielectric used as a matching layer in the proposed work, sandwiched between the prism and the BP layer. It acts as an insulating layer to prevent oxidation in the case of the BP layer. It has been widely used in sensing applications [16]. It has a low RI of 1.34 (633 nm) [18]. Its main component is fluorine, developed by a Japanese company (Asahi Glass Company). It is highly resistant to corrosion and chemicals and highly stable and has a waterproof feature. It also has applications in electronic devices like Field Effect Transistors (FETs) [13, 37]. So, the main objective of this proposed study is to numerically analyze the performance of an LRSPR-based biosensor using two different prisms. The performance parameters are computed and compared with the earlier SPR-based literature to convey the proposed work's merits.

Section 2 gives the design and theoretical modeling of the proposed LRSPR sensor. Section 3 gives the fabrication possibilities and error for the suggested LRSPR sensor

designs. Section 4 contains the numerical modeling. Section 5 composed of the results and discussions for the proposed sensor. At last, Section 6 concludes the current work.

2. Design and Theoretical Modeling

For the two different coupling prisms, 2S2G and BK7-based, two designs of LRSPR sensors have been shown in Figure 1. Figure 1(a) shows the labeled diagram of the proposed 2S2G prism/Cytop/Ag/BP-based LRSPR sensor and Figure 1(b) for the proposed BK7 prism/Cytop/Ag/BP.

The coupling prisms chosen for our design are chalcogenide (2S2G) and BK7. Its high refractive index (RI) impresses SPs to excite and raise the input wave's wave vector to match the surface plasmon wave vector (SPWV). The
RI of the 2S2G prism is taken as [38]

$$n_{2S2G} = \frac{2{:}693 \times 10^{-2}}{\lambda^4} + \frac{8{:}08 \times 10^{-3}}{\lambda^2} + \delta 1 \text{Þ} + 2{:}24047$$

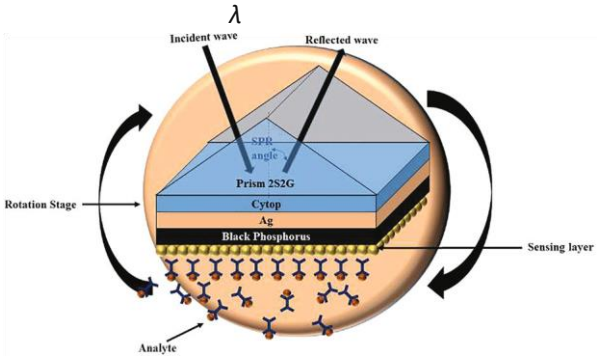

(a)

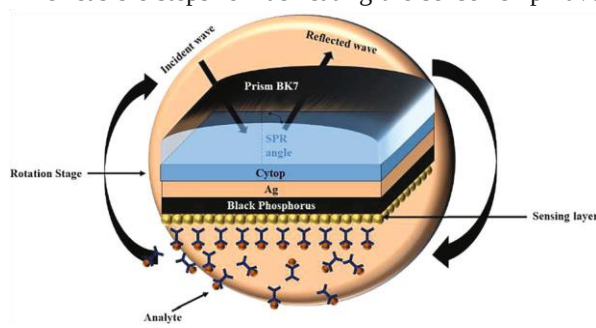

(b)

Figure 1: Proposed LRSPR sensor designs using (a) 2S2G prism and (b) BK7 prism.

Table 1: Layer parameters used in the current work at 633 nm.

Layer number	Materials used	Thickness (nm)	RI
First	2S2G prism/BK7 prism	—	2.358/1.5151
Second	Cytop	$D_2 = 2200$	1:34
Third	Ag	$D_3 = 15$	$0{:}056253 + i * 4{:}2760$
Fourth	BP	$D_4 = B * 0{:}5$, B = no. of BP layers	$3{:}531 - \text{i} * 0{:}04087$
Fifth	Sensing layer	—	$1{:}33 + \Delta n$ (Δn change in RI)

For the BK7 prism, its RI is given by [24]

$$n_{BK7} = \sqrt{1 + \frac{1{:}03961212\lambda^2}{\lambda^2 - 0{:}00600069867} + \frac{0{:}231792344\lambda^2}{\lambda^2 - 0{:}0200179144} + \frac{1{:}01046945\lambda^2}{\lambda^2 - 103{:}560653}} \quad \delta 2\text{Þ}$$

Here, λ is the operating wavelength of 633nm. The design parameters for other layers used in this proposed work have been summarized here in Table 1. Employing the Drude-Lorentz equation, for the Ag metal layer, its dielectric constant is given by [39]

$$\epsilon_{Ag} = \left(1 - \frac{\left(\lambda^2 * \lambda_c\right)}{\lambda_p^2}\right) : \quad \delta 3\text{Þ}\ \lambda_p \delta \lambda_c + \lambda *$$

$i\text{Þ}$

$\lambda_p$and λ_c are the plasma and collision wavelengths. The values of $\lambda_p = 0{:}14541\ \mu$m and $\lambda_c = 17{:}614\mu$m are taken, respectively.

3. Fabrication Possibilities and Errors

The feasible steps for fabricating the sensor chip have been given in this section. The coupling glass prism was cleaned up to 4-5 times with a solution having acetone vapor and deionized water. Then, it is coupled to the layer of Cytop and silver layer. Above the prism, the Cytop layer (dielectric) deposition must be done using the spin-coating method [40]. Then, the physical vapor deposition of silver metal is done by the thermal evaporator system over the Cytop layer [41].

Table 2: Sensitivity, FWHM, DA, and Q of the proposed LRSPR sensor designs with various fabrication errors.

Layer thickness (nm)	Fabrication errors	
	Computed parameters with variations of -10%	Computed parameters with variations of +10%
Ag, Cytop, BP (2S2G design)	S = 13:33, FWHM = 0:00527, DA = 189:7533, Q = 2529:41	S = 13:33, FWHM = 0:0054, DA = 185:18, Q = 2468:44
Ag, Cytop, BP (BK7 design)	S = 40, FWHM = 0:02, DA = 50, Q = 2000	S = 33:33, FWHM = 0:01, DA = 100, Q = 3333

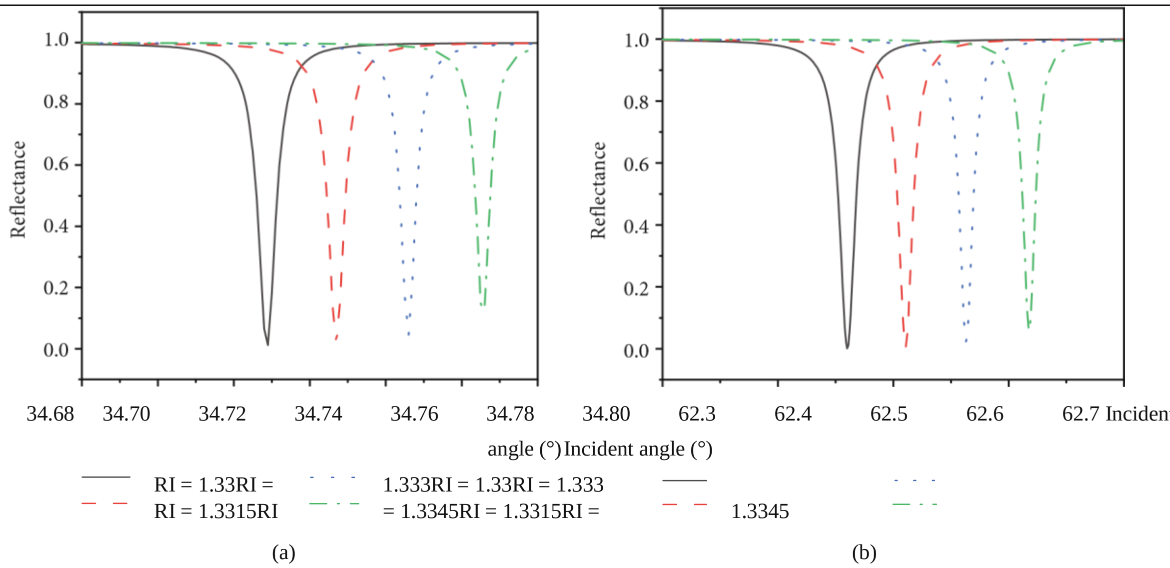

Figure 2: Reflectance of the proposed biosensor w.r.t. the incident angle by varying the RI of the sensing layer, for (a) 2S2G prism and (b) BK7 prism.

Then, the BP layer's fabrication was performed using a chemical vapor deposition (CVD) [35]. Next, this BP nanolayer shifted over the silver layer. As the fabrication process completes, these multilayers of chips are transferred to the prism. Finally, using the sensor setup, the output results are calculated. There are three main steps of the sensing mechanism: initially, firmly attach the sample cell to the detecting structure's surface; then control the analyte with a pump so that it flows slowly through the sample cell; at last, identify the flow of the analyte through the sample cell; a resonance signal is employed.

The fabrication errors were computed by varying all layer thicknesses by 10%. For RI = 1:345, the proposed design's performance parameters have been calculated, including the various fabrication errors. Table 2 shows the calculated values of the performance parameter for the proposed work.

4. Numerical Modeling

The TMM, without any approximations and great efficiency, was generally employed for reflectance calculation [42]. Using an N-layer matrix, a theoretical study was conducted here. For the kth layer, the dielectric constant (ϵ_K), thickness (d_K), and the RI are all defined. Using a characteristic matrix, the N-layer structure can be symbolized as [43]

$$P = \prod_{K=2}^{n-1} P_K = \begin{bmatrix} P_{11} & P_{12} \\ P_{21} & P_{22} \end{bmatrix} = \prod_{k=2}^{n-1} \begin{bmatrix} \cos(\alpha_K) & -i\sin(\alpha_K)/q_K \\ -iq_K\sin(\alpha_K) & \cos(\alpha_K) \end{bmatrix}. \quad (4)$$

Here, α_K, optical admittance $= d_K \Upsilon_0 \sqrt{\epsilon_K - n_2 \sin^2 \vartheta}$ and q_K, phase factor $= \sqrt{\epsilon_K - n_2 \sin^2 \vartheta}/\epsilon_K$, where ϑ, Υ_0, and ϵ_K represent the angle of incidence, wave number in free space, and kth layer's permittivity.

Finally, the reflectance for a p-polarized wave is expressed by [44]

$$R_p = r_p = \frac{2\left(P_{11} + \left(P_{12}q_n\right)\right)q_1 - \left(P_{21} + P_{22}q_n\right)}{\left(P_{11} + P_{12}q_n\right)q_1 + \left(P_{21} + P_{22}q_n\right)}. \quad (5)$$

4.1. Performance Parameter Calculation. An SPR sensor's performance can be well summarized using various performance parameters [45]. These parameters have been calculated after plotting the SPR curves.

The alteration in the RI of the sensing layer (Δn) gives rise to variation in the angle of resonance $(\Delta\vartheta)$. This factor is known as sensitivity (S). Therefore, sensitivity (S) can be expressed as follows: $S = \Delta\vartheta/\Delta n$, expressed in degree/RIU. Another parameter defining the sensor's performance is the full-width half maximum. It gives the variation of the incident angle at 50% reflectance. It can be expressed as follows: $\mathrm{FWHM} = \vartheta_2 - \vartheta_1$, expressed in degree $(°)$, where ϑ_2 and ϑ_1 are the angles at 50% reflectance. The detection accuracy parameter gives information about the sensor's detection exactness. It can be expressed as: $\mathrm{DA} = (\mathrm{FWHM})^{-1}$, expressed in (degree^{-1}). The next performance parameter is the quality factor or figure of merit (Q or FOM). Its expression is as follows: Q or $\mathrm{FOM} = S * \mathrm{DA}$, expressed in (1/RIU). The desired values for S, DA, and Q should be large, and for FWHM, it should be low [46].

4.2. Field Distribution Computation within the Layers. Using the TM polarized input radiation's reflectivity and transmittance, the electric field and magnetic field distribution components (E and H) in between the layers are generally written using the total characteristic matrix as [47]

$$\begin{bmatrix} -HE_{yx1}(z) \\ 1 \end{bmatrix} = P_1(z)\begin{bmatrix} q_1 \\ 1 \end{bmatrix} + \begin{bmatrix} -r_p \\ r_p \end{bmatrix} H_{y\mathrm{inc}}, \quad z_1 \le z \le z_2: \quad (6)$$

Here, H^{inc}_y and r_p denote the amplitude of the incident magnetic field and the reflectance coefficient, respectively.

Also,

$$P_1(z) = \begin{bmatrix} \cos\left(\beta_{k\,at\,z(1)}\right) & \left(i/q_1\right)\sin\left(\beta_{k\,at\,z(1)}\right) \\ iq_1\sin\left(\beta_{k\,at\,z(1)}\right) & \cos\left(\beta_{k\,at\,z(1)}\right) \end{bmatrix}. \quad (7)$$

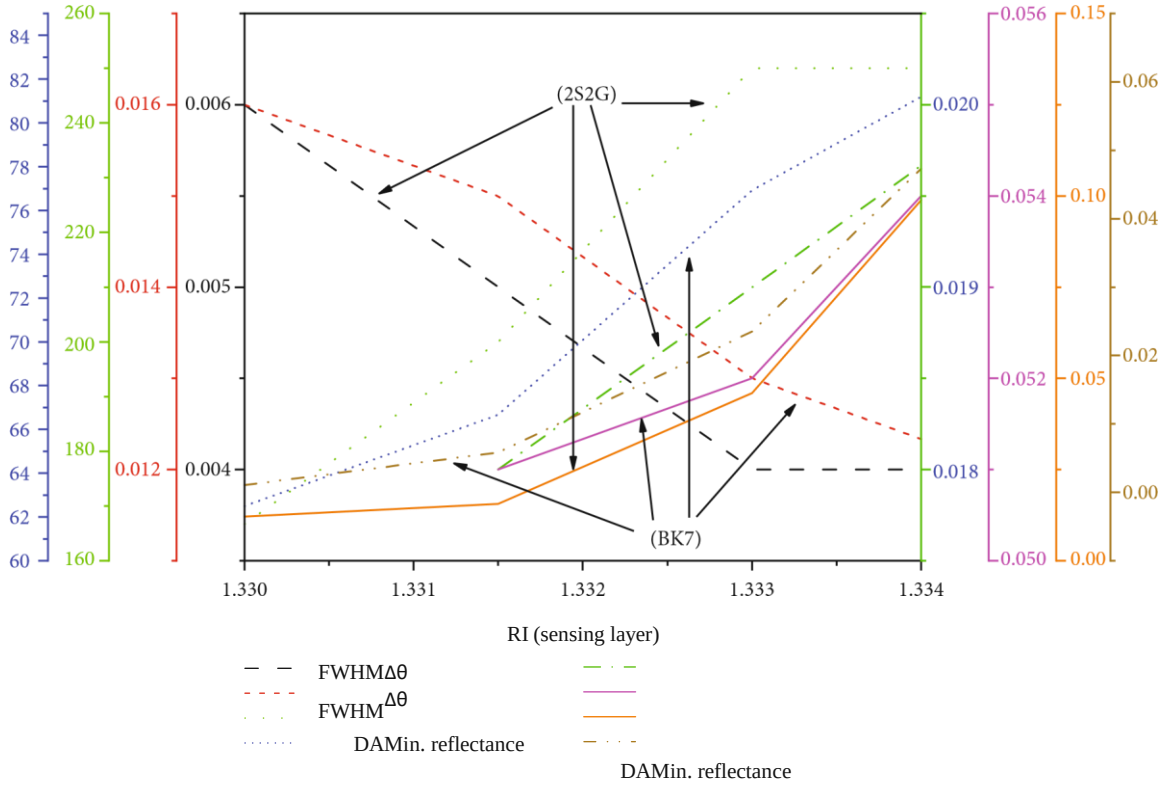

Figure 3: Alteration in FWHM, DA, $\Delta\vartheta$, and minimum reflectance as a function of RI of sensing layer for both 2S2G-based prism design and BK7-based prism design.

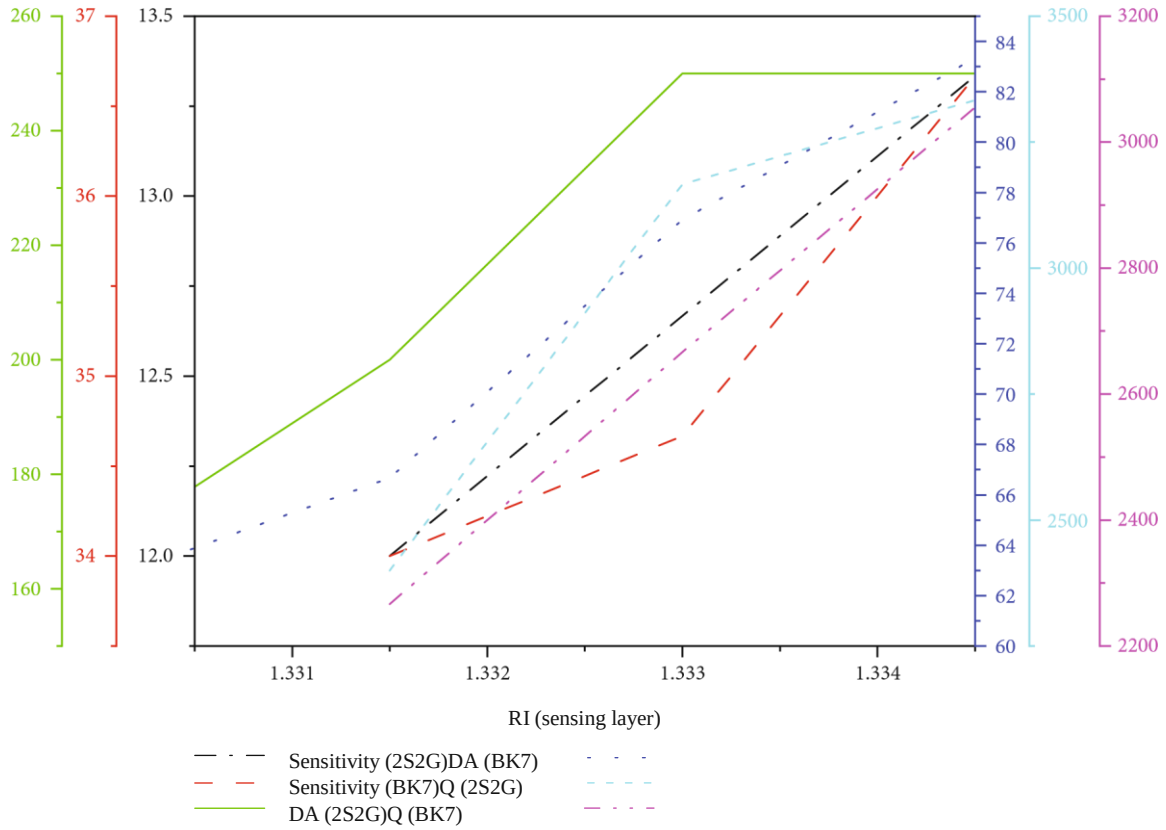

Figure 4: Sensitivity, DA, and Q plots w.r.t. the RI of the sensing layer for both designs.

Table 3: For 2S2G and BK7 designs: minimum reflectance, $\Delta\vartheta$, FWHM, DA, S, and Q value tabulation.

RI (sensing layer)	Proposed designs	Minimum reflectance	Change in SPR angle ($\Delta\vartheta$) (degree)	FWHM (degree)	DA (degree^{-1})	S (degree/RIU)	Q (RIU^{-1})
1.33	Design 1 (2S2G + Cytop + Ag + BP)	0.01207	Ref	0.006	166.66	Ref	2400
1.3315		0.01554	0.018	0.005	200	12	
1.333		0.04595	0.019	0.004	250	12.66667	3166.66
1.3345		0.12525	0.02	0.004	250	13.33333	3333.25
1.33	Design 2 (BK7 + Cytop + Ag + BP)	0.00105	Ref	0.016	62.5	Ref	2266.64
1.3315		0.00585	0.051	0.015	66.66667	34	
1.333		0.02349	0.052	0.013	76.92308	34.66667	2666.61
1.3345		0.05918	0.055	0.012	83.33333	36.66667	3055.48

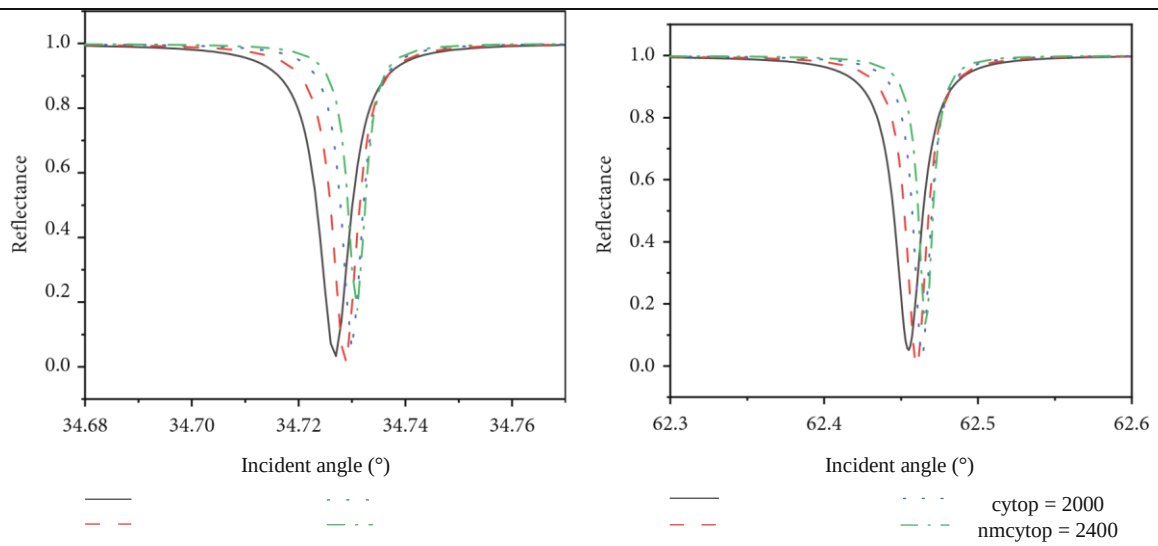

Figure 5: Effect of different thicknesses of Cytop layer and incidence angle on the reflectance for (a) 2S2G-based design and (b) BK7-based design.

For

$$2\ H^{yj}\eth\ Þ_{z}\ 3 \qquad 1$$

$$j \geq 2, 4- \qquad 5 = P_j\eth\ Þz * {}^{Y}{}_{j-1}\ P\ z\eth = z_i + d_i{}^{Þ}$$

$$2\ E1 + x_j\eth\ Þ_Z r_p\ 3H_{incy}\ ,\ z_j \leq z \leq z_{j+1}: \qquad \eth 8Þ$$

$$*$$

$$4q_1\ 1 - r_p\ 5$$

Here,

$$P_j\eth\ Þz = 2466iq\cos_j\ \sin\delta\theta_{k\ at\ z\eth k\ at\ z\eth\ =z=-zj-Þj Þ}\ q_{ij}\cos\sin\delta\theta_{k\ at\ z\eth k\ at\ z\eth\ =z=-zj-Þj Þ}3757:$$

$$\eth^{9}Þ$$

Here, $P_j\eth zÞ$, $E_{xj}\eth zÞ$, and $H_{yj}\eth zÞ$ indicate the propagation matrix, electric fields, and magnetic fields, respectively.

Table 4: Minimum reflectance computation for different thicknesses of Cytop.

Cytop thickness	Minimum reflectance (BK7 design)
2000 nm	0.05159
2200 nm	0.00105
2400 nm	0.03316
2600 nm	0.12938

5. Results and Discussions

The results of the proposed work have been explained for both the prism's configurations. Under the TM mode of input p-polarized light, the LRSPR signals can be excited using the two proposed biosensor setups.

At an operating wavelength of 633 nm, the reflectance curves have been studied with the RI alteration of the sensing layer for both the proposed biosensor configurations. Figures 2(a) and 2(b) show the impact of RI variation of the sensing layer and incidence angle on reflectance. The RI variation range has been considered from 1.330 to 1.3345 with a change of 0.0015. It has been observed that the lowest minimum reflectance values for both the designs (2S2G and BK7) are 0.01207 at 34.729 degree and 0.00105 at 62.46 degree, respectively. These values are very close to zero, which signifies that the maximum number of SPs gets excited, giving the proposed sensor's best performance (efficient and accurate).

The FWHM, DA, $\Delta\vartheta$, and minimum reflectance plots have been plotted combinedly for the proposed designs (Figure 3). The combined sensitivity, DA, and Q plots for both designs have been plotted in Figure 4. The minimum and maximum sensitivities for a design using a 2S2G prism have been calculated as 12 degree/RIU and 13.33 degree/RIU. For the BK7-based design, the maximum and minimum sensitivity values are calculated as 36.66 degree/RIU and 34 degree/RIU, respectively. The quality factor (Q), or FOM, is an important parameter for analyzing a sensor's performance. The plots for both designs giving the impact of RI of the sensing layer on the Q of the proposed sensor have been shown. The maximum value of Q is desired for the good performance of the sensor. So, the maximum Q values computed here are 3333.25 RIU^{-1} and 3055.5 RIU^{-1} for the 2S2G design and BK7 design, respectively. The value of RI of the sensing layer varies from 1.33 to 1.3345, with a variation of 0.0015. The parameters like FWHM, DA, S, and Q, along with the minimum reflectance and change in SPR angle values computed for both designs, have been shown in Table 3.

Table 5: Comparison table with the current and previously reported prism-coupled SPR sensors.

Layer designs	Q (maximum)	DA (maximum)	Reference
2S2G prism, Cytop, Ag, BP, sensing layer (Design1)	3333.25	250	Current
BK7 prism, Cytop, Ag, BP, sensing layer (Design 2)	3055.5	83.33	Current
2S2G, Cytop, Au, antimonene, BRE, sensing layer	1960	100	[48]
BK7 prism, dielectric, GZO, sensing layer	150	—	[49]
BK7 prism, DBL, MXene, FG, sensing layer	347	—	[32]
BK7 prism, MXene, sensing layer	304	—	[50]
Prism, Ag, Ne, sensing layer	312.3	—	[51]

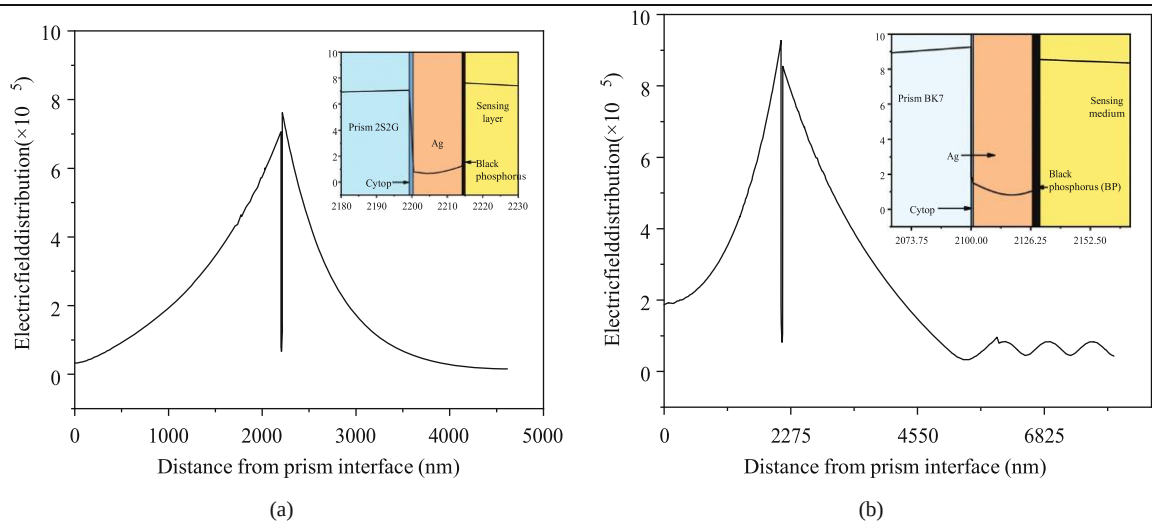

Figure 6: The electric field distribution as a function of perpendicular distance from the prism interface for (a) 2S2G design and (b) BK7 design.

After these calculations, the observation is that the DA and Q values are greater for the 2S2G design than for another prism (BK7) design, although in terms of sensitivity, the BK7-based proposed sensor design is more sensitive than the other one.

The Cytop layer's thickness impact has now been investigated on the reflectance at RI = 1:33. From both plots of Figure 5, it has been seen that for the Cytop thickness of 2200 nm, the minimum reflectance we are getting is 0.01207 (for 2S2G design) and 0.00105 (for BK7 design), respectively. So, the optimized thickness value has been considered 2200nm. For the 2S2G prism-based design, as the Cytop thickness increases from 2000 nm to 2200 nm, the minimum reflectance value shifts from 0.03278 to 0.01207. Then by further enhancing the thickness to 2400nm, the minimum reflectance value reaches 0.05542. The final value of reflectance reaches 0.17463 for a thickness of 2600nm. Similarly, for the proposed BK7-based design, the corresponding minimum reflectance values have been shown in Table 4.

A comparison between the past research work and the proposed work has now been made here in Table 5. The analysis shows our proposed design's performance enhancement in terms of quality factor and DA.

Figure 6 shows the tangential electric field distribution plots for both proposed designs with the 2S2G and BK7 prisms. The variation of field distribution with the distance from the first interface of 2S2G prism and Cytop layer to the last interface of BP layer and sensing layer varies from 0 to 2180 nm. The inset figure (Figure 6(a)) shows the zoomed-up view of the interfaces shown by the oval circle. The distance varying is from 2180 nm to 2230 nm. Similarly, for the BK7 design, the distance from the coupling BK7 prism and Cytop layer's first interface to the BP layer's and sensing layer's last interface varies from 0 to 2273 nm. The inset figure (Figure 6(b)) shows the zoomed-up view of the interfaces shown in the oval circle. The distance varying is from 2060 nm to 2163 nm.

The factor which defines how much the electric field is effectively concentrated in the vicinity of the BP and sensing layer's last interface is the Electric Field Intensity Enhancement Factor (EFIEF). Both electric and magnetic fields are involved in computing the EFIEF parameter. Mathematically, its expression is given as [52]

$$E_{\parallel}\tilde{\eth}N_{E_{\parallel}}/\tilde{\eth}\tilde{\eth}1^{N}/2\text{Þ}\,\text{Þ}\text{Þ} = \frac{\epsilon_1}{\epsilon_n}\frac{H_{y\parallel}}{H\tilde{\eth}N_{y\parallel}/\tilde{\eth}\tilde{\eth}1^{N}/2^{-}\text{Þ}}\,1\text{Þ}\text{Þ}^{2}\text{:}\;\tilde{\eth}10\text{Þ}$$

6. Conclusion

Two different coupling prisms (2S2G and BK7) have been used in this novel work to design two LRSPR sensors using the Cytop/Ag/BP as other layers. The principle followed in this study is the attenuated total reflection method. The transfer matrix method has been employed for reflectance computation. The proposed design's performance in different performance parameters has been carried out. The earlier results signify that our proposed sensor designs provide better Q of 3333.25 RIU^{-1} and 3055.5 RIU^{-1} for 2S2G/Cytop/Ag/BP design and another design consisting of BK7/Cytop/Ag/BP, respectively, and the DA values 250 $degree^{-1}$ and 83.33 $degree^{-1}$ have been calculated. The structure that uses the BK7 prism shows a greater sensitivity of 36.66 degree/RIU. So, we believe that the proposed LRSPR sensor designs open a new window for promising and adaptable sensors in the future.

Data Availability

Data underlying the results presented in this paper are not publicly available at this time but may be obtained from the authors upon reasonable request.

Conflicts of Interest

The authors declare no conflicts of interest.

References

[1] A. Shalabney and I. Abdulhalim, "Sensitivity-enhancement methods for surface plasmon sensors," *Laser & Photonics Reviews*, vol. 5, no. 4, pp. 571–606, 2011.

[2] S. Jain, A. Paliwal, V. Gupta, and M. Tomar, "Refractive index tuning of SiO_2 for long range surface plasmon resonance based biosensor," *Biosensors & Bioelectronics*, vol. 168, article 112508, 2020.

[3] W. Bu, Z. Wu, P. P. Shum, X. Shao, and J. Pu, "Sensitivity enhanced refractive index fiber sensor based on long-range surface plasmon resonance in SiO_2-Au-TiO_2 heterostructure," *Photonics*, vol. 8, no. 9, p. 379, 2021.

[4] A. Pal and A. Jha, "A theoretical analysis on sensitivity improvement of an SPR refractive index sensor with graphene and barium titanate nanosheets," *Optik*, vol. 231, article 166378, 2021.

[5] X. Yang, Y. Yuan, Z. Dai, F. Liu, and J. Huang, "Optical property and adsorption isotherm models of glucose sensitive membrane based on prism SPR sensor," *Sensors and Actuators B: Chemical*, vol. 237, pp. 150–158, 2016.

[6] A. Bijalwan and V. Rastogi, "Sensitivity enhancement of a conventional gold grating assisted surface plasmon resonance sensor by using a bimetallic configuration," *Applied Optics*, vol. 56, no. 35, pp. 9606–9612, 2017.

[7] P. Kumar and R. S. Kaler, "Multilayer with periodic grating based high performance SPR waveguide sensor," *Optics Communications*, vol. 395, pp. 154–158, 2017.

[8] Y. Singh and S. K. Raghuwanshi, "Titanium dioxide (TiO_2) coated optical fiber-based SPR sensor in near-infrared region with bimetallic structure for enhanced sensitivity," *Optik*, vol. 226, article 165842, 2021.

[9] T. Kaminski, A. Gunnarsson, and S. Geschwindner, "Harnessing the versatility of optical biosensors for target-based small-molecule drug discovery," *ACS Sensors*, vol. 2, no. 1, pp. 10–15, 2017.

[10] S. Neethirajan, V. Ragavan, X. Weng, and R. Chand, "Biosensors for sustainable food engineering: challenges and perspectives," *Biosensors*, vol. 8, no. 1, p. 23, 2018.

[11] C. Hu, N. Gan, Y. Chen, L. Bi, X. Zhang, and L. Song, "Detection of microcystins in environmental samples using surface plasmon resonance biosensor," *Talanta*, vol. 80, no. 1, pp. 407–410, 2009.

[12] P. Damborský, J. Švitel, and J. Katrlík, "Optical biosensors," *Essays in Biochemistry*, vol. 60, no. 1, pp. 91–100, 2016.

[13] J. Jing, Q. Wang, W. Zhao, and B. Wang, "Long-range surface plasmon resonance and its sensing applications: a review," *Optics and Lasers in Engineering*, vol. 112, no. 2018, pp. 103– 118, 2019.

[14] D. Sarid, "Long-range surface-plasma waves on very thin metal films," *Physical Review Letters*, vol. 47, no. 26, pp. 1927–1930, 1981.

[15] A. Uniyal, B. Chauhan, A. Pal, and Y. Singh, "Surface plasmon biosensor based on Bi_2Te_3antimonene heterostructure for the detection of cancer cells," *Applied Optics*, vol. 61, no. 13, pp. 3711–3719, 2022.

[16] L. Wu, K. Che, Y. Xiang, and Y. Qin, "Enhancement of sensitivity with high-reflective-index guided-wave nanomaterials for a long-range surface plasmon resonance sensor," *Nanomaterials*, vol. 12, no. 1, 2022.

[17] N. Liu, S. Wang, Q. Cheng, B. Pang, and J. Lv, "High sensitivity in Ni-based SPR sensor of blue phosphorene/transition metal dichalcogenides hybrid nanostructure," *Plasmonics*, vol. 16, no. 5, pp. 1567–1576, 2021.

[18] M. Kumar, K. B. Thapa, and P. Singh, "Long-range surface plasmon resonance biosensors with cytop/Al/perovskite and cytop/Al/MoS_2 configurations," *Physica Scripta*, vol. 97, no. 5, article 055501, 2022.

[19] Y. Kumar, R. Mishra, E. Panwar, J. Kaur, and R. Panwar, "Design, optimization and critical analysis of graphene based surface plasmon resonance sensor for DNA hybridization," *Optical and Quantum Electronics*, vol. 51, no. 10, p. 343, 2019.

[20] O. Krupin, H. Asiri, C. Wang, R. N. Tait, and P. Berini, "Biosensing using straight long-range surface plasmon waveguides," *Optics Express*, vol. 21, no. 1, pp. 698–709, 2013.

[21] H. Yu, Y. Peng, Y. Yang, and Z. Y. Li, "Plasmon-enhanced light-matter interactions and applications," *npj Computational Materials*, vol. 5, no. 1, pp. 1–14, 2019.

[22] B. Karki, A. Uniyal, B. Chauhan, and A. Pal, "Sensitivity enhancement of a graphene, zinc sulfide-based surface plasmon resonance biosensor with an Ag metal configuration in the visible region," *Journal of Computational Electronics*, vol. 21, no. 2, pp. 445–452, 2022.

[23] E. Kretschmann and H. Raether, "Notizen: radiative decay of non radiative surface plasmons excited by light," *Zeitschrift für Naturforschung*, vol. 23, no. 12, pp. 2135-2136, 1968.

[24] S. Gan, Y. Zhao, X. Dai, and Y. Xiang, "Sensitivity enhancement of surface plasmon resonance sensors with 2D franckeite nanosheets," *Results in Physics*, vol. 13, article 102320, 2019.

[25] A. Otto, "Excitation of nonradiative surface plasma waves in silver by the method of frustrated total reflection," *Zeitschrift Für Physik A Hadrons And Nuclei*, vol. 216, no. 4, pp. 398–410, 1968.

[26] D. Hou, X. Ji, N. Luan et al., "Surface plasmon resonance sensor based on double-sided polished microstructured optical fiber with hollow core," *IEEE Photonics Journal*, vol. 13, no. 4, pp. 1–8, 2021.

[27] Y. Guo, N. M. Singh, C. M. das et al., "Two-dimensional $PtSe_2$ theoretically enhanced Goos-Hänchen shift sensitive plasmonic biosensors," *Plasmonics*, vol. 15, no. 6, pp. 1815–1826, 2020.

[28] A. W. Wark, H. J. Lee, and R. M. Corn, "Long-range surface plasmon resonance imaging for bioaffinity sensors," *Analytical Chemistry*, vol. 77, no. 13, pp. 3904–3907, 2005.

[29] M. Khodami and P. Berini, "Biomolecular kinetics analysis using long-range surface plasmon waveguides," *Sensors and Actuators B: Chemical*, vol. 243, pp. 114–120, 2017.

[30] Y. Wang, W. Knoll, and J. Dostalek, "Bacterial pathogen surface plasmon resonance biosensor advanced by long range surface plasmons and magnetic nanoparticle assays," *Analytical Chemistry*, vol. 84, no. 19, pp. 8345–8350, 2012.

[31] D. Fan, L. Wu, Z. Ling, L. Jiang, J. Guo, and X. Dai, "Optically integrated InP–Si_3 N_4 hybrid laser," *IEEE Photonics Journal*, vol. 8, no. 6, pp. 1–11, 2016.

[32] P. S. Pandey, Y. Singh, and S. K. Raghuwanshi, "Theoretical analysis of the LRSPR sensor with enhance FOM for low refractive index detection using MXene and fluorinated graphene," *IEEE Sensors Journal*, vol. 21, no. 21, pp. 23979–23986, 2021.

[33] L. Li, Y. Yu, G. J. Ye et al., "Black phosphorus field-effect transistors," *Nature Nanotechnology*, vol. 9, no. 5, pp. 372–377, 2014.

[34] P. Chen, N. Li, X. Chen, W. J. Ong, and X. Zhao, "The rising star of 2D black phosphorus beyond graphene: synthesis, properties and electronic applications," *2D Materials*, vol. 5, no. 1, article 014002, 2018.

[35] J. B. Smith, D. Hagaman, and H. F. Ji, "Growth of 2D black phosphorus film from chemical vapor deposition," *Nanotechnology*, vol. 27, no. 21, pp. 215602–215608, 2016.

[36] Y. Singh and S. K. Raghuwanshi, "Sensitivity enhancement of the surface plasmon resonance gas sensor with black phosphorus," *IEEE Sensors Letters*, vol. 3, no. 12, pp. 1–4, 2019.

[37] W. Huang, K. Besar, R. LeCover et al., "Label-free brain injury biomarker detection based on highly sensitive large area organic thin film transistor with hybrid coupling layer," *Chemical Science*, vol. 5, no. 1, pp. 416–426, 2014.

[38] P. K. Maharana and R. Jha, "Chalcogenide prism and graphene multilayer based surface plasmon resonance affinity biosensor for high performance," *Sensors and Actuators B: Chemical*, vol. 169, pp. 161–166, 2012.

[39] A. K. Sharma and B. D. Gupta, "On the performance of different bimetallic combinations in surface plasmon resonance based fiber optic sensors," *Journal of Applied Physics*, vol. 101, no. 9, article 093111, 2007.

[40] C. Liu, Y. Li, M. V. Lee, A. Kumatani, and K. Tsukagoshi, "Selfassembly of semiconductor/insulator interfaces in one-step spin-coating: a versatile approach for organic field-effect transistors," *Physical Chemistry Chemical Physics*, vol. 13, no. 21, pp. 7917–7933, 2015.

[41] M. F. O. Hameed and S. Obayya, *Computational Photonic Sensors*, Springer, 2019.

[42] P. Varasteanu, "Optimizing the tin selenide (SnSe) allotrope/ gold-based surface plasmon resonance sensors for enhanced sensitivity," *Plasmonics*, vol. 16, no. 2, pp. 341–347, 2021.

[43] A. Uniyal, A. Pal, and B. Chauhan, "Long-range Spr sensor employing platinum diselenide and cytop nanolayers giving improved performance," *Physica B: Condensed Matter*, vol. 649, article 414487, 2023.

[44] K. Jindal, M. Tomar, R. S. Katiyar, and V. Gupta, "N-doped ZnO thin film for development of magnetic field sensor based on surface plasmon resonance," *Optics Letters*, vol. 38, no. 18, pp. 3542–3545, 2013.

[45] A. Uniyal, B. Chauhan, A. Pal, and V. Srivastava, "InP and graphene employed surface plasmon resonance sensor for measurement of sucrose concentration: a numerical approach," *Optical Engineering*, vol. 61, no. 5, pp. 1–13, 2022.

[46] B. Karki, B. Vasudevan, A. Uniyal, A. Pal, and V. Srivastava, "Hemoglobin detection in blood samples using a graphenebased surface plasmon resonance biosensor," *Optik*, vol. 270, article 169947, 2022.

[47] A. Shalabney and I. Abdulhalim, "Electromagnetic fields distribution in multilayer thin film structures and the origin of sensitivity enhancement in surface plasmon resonance sensors," *Sensors and Actuators, A: Physical*, vol. 159, no. 1, pp. 24–32, 2010.

[48] N. Pal, J. Bahadur, M. Yogendra, and K. Prajapati, "Longrange SPR imaging sensor mediated by antimonene for biomolecule sensing with ultrahigh imaging sensitivity and figure of merit," *Plasmonics*, vol. 17, no. 4, pp. 1571– 1580, 2022.

[49] B. Ruan, Q. You, J. Zhu et al., "Improving the performance of an SPR biosensor using long-range surface plasmon of Gadoped zinc oxide," *Sensors*, vol. 18, no. 7, 2018.

[50] X. Dai, C. Song, C. Qiu, L. Wu, and Y. Xiang, "Theoretical investigation of multilayer $Ti_3C_2T_x$MXene as the plasmonic material for surface plasmon resonance sensors in near infrared region," *IEEE Sensors Journal*, vol. 19, no. 24, pp. 11834– 11838, 2019.

[51] G. Lan, S. Liu, X. Zhang, Y. Wang, and Y. Song, "A simplified high figure-of-merit prism-free surface plasmon resonance refractive index sensor based on self adaptive angular interrogation," *Review of Scientific Instruments*, vol. 86, article 025006, 2015.

[52] A. Panda and P. D. Pukhrambam, "Modeling of highperformance SPR refractive index sensor employing novel 2D materials for detection of malaria pathogens," *IEEE Transactions on Nanobioscience*, vol. 21, pp. 312–319, 2022.